# Facile Preparation of Lightweight and Flexible PVA/PEDOT:PSS/MWCNT Ternary Composite for High-Performance EMI Shielding in the X-Band Through Absorption Mechanism

M. JASNA,[1] NEERAJ K. PUSHKARAN,[2] M. MANOJ,[1] C.K. AANANDAN,[2,3,4] and M.K. JAYARAJ (ORCID)[1,3,4,5]

1.—Department of Physics, Cochin University of Science and Technology, Kochi, Kerala 682 022, India. 2.—Department of Electronics, Cochin University of Science and Technology, Kochi, Kerala 682 022, India. 3.—Centre of Excellence in Advanced Materials, Cochin University of Science and Technology, Kochi, Kerala 682 022, India. 4.—Inter University Centre for Nanomaterials and Devices, Cochin University of Science and Technology, Kochi, Kerala 682 022, India. 5.—e-mail: mkj@cusat.ac.in

Electromagnetic safeguards are key factors for electronic devices. Lightweight and highly flexible polymer composite films with high electrical conductivity are considered to be efficient electromagnetic interference (EMI) shielding materials. Polymer composites offer alternative to metal-based composites which have poor flexibility, corrodibility, and are difficult to process. Here, highly flexible polyvinyl alcohol/poly (3, 4-ethylenedioxythiophene):polystyrene sulfonate/multiwalled carbon nanotube (PVA/PEDOT:PSS/MWCNT) free-standing composite films were fabricated by a solution mixing process followed by a simple solvent casting technique. PVA/PEDOT:PSS/MWCNT composite films of thickness around 20 microns showed high EMI shielding effectiveness (SE) in the X-band over the frequency range of 8–12 GHz. Incorporation of MWCNT into the polymer matrix considerably increased the mechanical strength of the PVA/PEDOT:PSS/MWCNT composite free-standing film. This investigation revealed that PVA/PEDOT:PSS/MWCNT composite film with 0.5 wt.% of MWCNT showed excellent absorption-dominated EMI SE of 60 dB over the frequency range of 8–12 GHz with extensive tensile strength. Our study opens a facile way to design flexible, lightweight and free-standing films as EMI shielding for next-generation flexible electronic devices.

**Key words:** EMI shielding, carbon nanotubes, conducting polymer, electrical conductivity

## INTRODUCTION

Electromagnetic radiation from electronic devices operating at high frequencies is very harmful to other highly sensitive electronic devices, as well as to human health. Electromagnetic interference (EMI) shielding is essential for suppressing or attenuating electromagnetic radiation induced by wireless communication and other devices. Consequently, EMI shielding materials capable of reducing electromagnetic radiation have received great attention in the research.[1–3] Even though metal-based composites are used as EMI shielding materials due to their higher electrical conductivity, these are often found to be unsuitable for EMI shielding when considering the weight, poor

mechanical flexibility, corrodibility, difficulty in processing, etc. Features such as mechanical flexibility or stretchability and light weight are very important for the practical applications of EMI shielding, especially in the fields of machinery, aerospace technology, aircraft and next-generation flexible and stretchable electronic systems.

EMI shielding effectiveness (SE) can be achieved by incorporating carbonaceous materials like carbon nanotubes (CNTs), graphene, fullerene, etc., into the polymer matrix. These polymer composites are lightweight, anti-corrosive, cost-effective and more flexible than metal-based shielding materials.[4–8] Among different carbonaceous materials, carbon nanotubes are very important due to their outstanding properties such as high electrical conductivity, mechanical strength (10–60 GPa) and high aspect ratio. Carbon nanotubes are a well-known material having a quasi-one-dimensional structure that consists of two or more graphene cylinders with interlayer separation, as in graphite. An enhancement in conductivity is observed at lesser filler loading (less than 1%) for CNTs.[9] The cross-linking nature of CNTs in the polymer matrix is used to form high strength composite materials. For instance, poly(dimethylsiloxane), butyl rubber and polyurethane based flexible composite films have been used as EMI shielding materials, with multi-walled carbon nanotubes (MWCNTs) or single walled carbon nanotubes (SWCNT) as conducting nanofillers in the polymer matrix. Recently, polymers such as poly(methyl methacrylate) (PMMA) coated MWCNT and nanoparticle decorated MWCNT or graphene polymer blends have been reported as EMI shielding materials in different frequency ranges with favorable EMI SE ($\sim$ 21–32 dB).[10–17] Moreover, many researchers focus on developing EMI shielding materials based on ferromagnetic particles of Fe, Ni, Co and their alloy polymer composites or carbon/ferromagnetic composites.[18,19] Intrinsically conducting polymers [polyaniline (PANI), polypyrrole (PPy), and poly(3,4 ethylenedioxythiophene) (PEDOT)] are another choice for EMI shielding materials due to their high conductivity, solution processability, low cost and light weight. Recent research is focused on conductive polymer composite foams with different conducting nanofillers such as graphene, CNTs and silver nanowires, which were found to excel as high-performance lightweight EMI shielding materials in the X-band region.[20–22] Conducting polymers are modeled as metallic islands immersed in a pool of insulators.[23] The role of the filler is to bridge these metallic islands, hence an interconnected network is formed and the transport mechanism is enhanced. Wu et al. created cellular-structured graphene foam (GF) with poly (3, 4-ethylenedioxythiophene):polystyrene sulfonate (PEDOT:PSS) conductive coating for low-density EMI shielding material.[20] They showed EMI SE of around 91 dB in the X-band region at a density of few milligrams

per cubic centimeter. Nevertheless synthesis procedure for the fabrication of the conductive composite foam is not suitable for large-scale industrial applications. On the basis of both light weight and cost-effective large area fabrication, conductive polymer composite free-standing flexible films have recently become prominent candidates for high-performance shielding materials. Table I represents the reported values of EMI performance of the polymer composite flexible films in the X-band. Hsiao et al. reported reduced graphene oxide/water-borne polyurethane lightweight and flexible composite prepared by a layer-by-layer self-assembly technique that showed an EMI SE of around 34 dB in the X-band.[24] Song et al. fabricated flexible all-carbon networks (carbon nanofiber–graphene nanosheet–carbon nanofiber) via electrospinning processing, and an EMI SE of $\sim$ 28 dB was achieved.[25]

Lightweight and easily foldable MWCNT/meso carbon microbead composite paper (0.15–0.6 mm thickness) was fabricated with EMI SE of 31–56 dB in the X-band frequency range.[26] Poly(vinylidene fluoride)/graphene/CNT composite flexible film with 3 wt.% of MWCNT at a thickness of 0.1 mm showed an EMI SE of $\sim$ 28 dB over the frequency range from 18.6 GHz to 26.5 GHz.[27] Li et al. reported CNT/PANI flexible films with specific shielding effectiveness of $7.5 \times 10^4$ dB cm$^2$ g$^{-1}$[28] polystyrene/poly(vinylidene fluoride)/MWCNT nanocomposite with SE of 19 dB was developed by Sultana et al.[29] Poly(dimethylsiloxane)/MWCNT and Fe$_3$O$_4$ films with thickness of 0.9 mm were fabricated with SE of $-$ 28 dB in the frequency range of 12–18 GHz.[30]

In previous reports, a high percentage of nanofillers were loaded in the polymer matrix and also, in many cases, complicated synthesis procedures have been followed to obtain composite materials as final products. The following criteria have emerged as important factors in compatibility between conducting nanofillers and a polymer matrix: (1) favorable interfacial integration, (2) homogenous dispersion to form conductive networks and (3) low loading of nanofillers to avoid aggregation.The solvent casting technique is widely used for fabricating free-standing polymer composite films by incorporating conducting nanofillers within the insulating polymer matrix. The main advantage of this technique is its support for large area fabrication. In CNT-based composite film, there is a chance of agglomeration of MWCNT due to its van der Waals force between the $\pi$–$\pi$ stacking, which results in poor performance of the composite film. In previous reports based on carbonaceous material polymer composites, some additives have been used to obtain homogenous dispersion of CNTs in the polymer matrix. High weight percentage of nanofillers have also been loaded to attain high EMI SE. For practical applications, PEDOT:PSS is the most successful conducting polymer, due to its aqueous dispersion and tunable electrical conductivity.

Facile Preparation of Lightweight and Flexible PVA/PEDOT:PSS/MWCNT Ternary Composite
for High-Performance EMI Shielding in the X-Band Through Absorption Mechanism

1691

**Table I. EMI performance of the polymer composite films in the X-band in the literature**

| Materials | Mechanical property | Thickness (mm) | EMI SE (dB) | References |
|---|---|---|---|---|
| Polyaniline/polyurethane | Flexible | 1.9 | $\sim 26$ | 33 |
| Polyaniline/nylon lycra fabrics | Flexible | – | $\sim 26$ | 34 |
| SWCNT/butyl rubber | Stretchable up to 1000% strain | 1 | 9–13 | 35 |
| MWCNT/poly(dimethylsiloxane) | Stretchable within 20% strain | – | $\sim 16$ | 36 |
| MWCNT/polyurethane | Flexible | 2.5 | $\sim 41.6$ | 37 |
| MWCNT/polyurethane | Flexible | 1.5 | $\sim 29$ | 38 |
| Graphene/polyetherimide | Flexible | 2.3 | $\sim 20$ | 39 |
| Graphene/Poly(dimethylsiloxane) | Flexible | 1 | $\sim 20$ | 40 |
| Waterborne/silver nanowire | Flexible | – | $\sim 20$ | 41 |
| rGO/waterborne polyurethane | Flexible | 2 | $\sim 32$ | 42 |
| rGO/waterborne polyurethane | Flexible | 1 | $\sim 34$ | 24 |
| Microcellular polyetherimide-graphene foams | | | $\sim 44$ | 39 |
| Few layered graphene/polyvinylalcohol composite | Flexible | 1 | $\sim 19.5$ | 43 |
| Graphene nanosheet/waterborne Polyurethane | Flexible | – | $\sim 38$ | 44 |
| PEDOT:PSS/Waterborne Polyurethane | Flexible | 0.15 | $\sim 62$ | 31 |
| PVA/PEDOT:PSS/MWCNT 0.5 wt.% (present work) | Flexible | 0.02 | $\sim 60.3$ | |

There are only a few reports on PEDOT:PSS based composite free-standing flexible films for EMI shielding applications. Li et al. prepared waterborne polyurethane (WPU)/PEDOT:PSS stretchable film of thickness 0.15 mm and showed an EMI SE of $\sim 62$ dB in the X-band at 20 wt.% of PEDOT:PSS.[31]

The present work is dedicated to the development of high performance EMI shielding materials which meet the following criteria: (1) flexible and lightweight shielding materials at a low fraction of nanofillers, (2) simple, cost-effective and large-scale fabrication strategy and (3) composite exhibiting very high EMI SE along with the criteria mentioned above for realizing next-generation portable/flexible electronics. We report a facile synthesis technique for the preparation of polyvinyl alcohol/poly (3, 4-ethylenedioxythiophene):polystyrene sulfonate/multiwalled carbon nanotube (PVA/PEDOT:PSS/MWCNT) in the form of a free-standing, flexible and lightweight ternary composite film. Polyvinyl alcohol (PVA) was chosen as the polymer matrix due to its water solubility, wide commercial availability, good flexibility, outstanding film forming and emulsifying properties.[32] It acts as inert polymer that assists uniform MWCNT dispersion through the polymer matrix. The role of PEDOT:PSS is that of a surfactant that minimizes the agglomeration of MWCNT in the polymer matrix and disperses MWCNTs uniformly without agglomeration, and also helps to increase the electrical conductivity of the composites. The use of PEDOT:PSS helps in the formation of interconnected MWCNT networks, even at a low fraction of MWCNT. Consequently, a combination of PEDOT:PSS with MWCNT reduces unadorned agglomeration and can make a good conducting composite film with low loading of MWCNTs. MWCNTs are incorporated not only for conductivity enhancement, but also to facilitate absorption of incoming microwave radiation. Usually, thick films (1–2 mm) show high EMI shielding by absorbing electromagnetic (EM) waves. Here, even the micron sized films showed better EMI SE than thick films. To the best of our knowledge, this is the first report presenting PVA/PEDOT:PSS/MWCNT shielding film of a few micrometers (20 $\mu$m) which exhibits excellent EMI SE (60 dB) even at a low fraction of MWCNTs (0.5 wt.%), making it stand out in the prevalent research domain of flexible shielding materials.

## EXPERIMENTAL

### Materials

MWCNT (diameter: 30–50 nm, length: $\sim 20$ $\mu$m, purity: > 95 wt.%) synthesized by chemical vapor deposition technique was supplied by Chengdu organic chemical Co. Ltd. PEDOT:PSS aqueous dispersion (1.3 wt.% in $H_2O$) was acquired from Sigma Aldrich. Dimethyl sulfoxide (DMSO) was obtained from Sigma Aldrich. Other chemicals used were of analytical grade.

## Preparation of Isopropyl Alcohol (IPA)/ MWCNT Solution

MWCNTs are bundled together by van der Waals force, and its hydrophobicity limits the uniform dispersion of the MWCNT. Hence, MWCNTs require some modification of their walls with suitable chemical treatment to enhance their dispersion in aqueous solution. For this, 0.5 g MWCNTs were dissolved in a mixture of (6 M) $H_2SO_4$:$HNO_3$ (6 M) in a volume ratio of 3:1 and refluxed at 120°C for 12 h. Purified MWCNTs were vacuum filtered using a membrane filter with pore size of 0.25 $\mu$m, then the material was washed with de-ionized water until it reached pH 7 and was dried overnight at 80°C in a vacuum oven. These functionalized MWCNTs were used for the preparation of composite films. Various amounts of functionalized MWCNTs (0.01 g, 0.05 g and 0.1 g) were dispersed in 5 ml isopropyl alcohol (IPA) and were ultrasonicated for 30 min, and again stirred for 1 h to get a homogeneously dispersed solution.

## Preparation of PEDOT:PSS/MWCNT Solution

Conducting polymer PEDOT:PSS with 0.625 weight ratio of PEDOT to PSS was used for the fabrication of composite films. The conductivity of the PEDOT:PSS can be improved by adding organic solvent DMSO. PEDOT:PSS solution (5 ml) were mixed with 5 vol.% of DMSO and were magnetically stirred for 2 h. This mixture was then added to the prepared MWCNT/IPA solution and ultrasonicated for another 2 h to get a uniform suspension of PEDOT:PSS/MWCNT. Here, PEDOT:PSS acted as surfactant for obtaining good dispersion of MWCNTs, and the process was termed as non-covalent functionalization.

## Fabrication of PVA/PEDOT:PSS/MWCNT Composite Free-Standing Films

Polyvinyl alcohol (PVA), a hydrophilic polymer, was selected as matrix for the fabrication of free standing films. Polyvinyl alcohol-based solution was prepared by adding 0.13 g PVA in 10 ml de- ionized water (1.3 wt.% PVA). The solution was magnetically stirred for 3 h at 60°C. The as-prepared homogenous PEDOT:PSS/MWCNT solution was mixed with the PVA solution and again ultrasonicated for 2 h to obtain a homogenous PVA/PEDOT:PSS/MWCNT solution. PVA is also a good candidate for better adhesion with the MWCNTs and acts as a macromolecular surfactant to assist MWCNT dispersion. PVA/PEDOT:PSS/MWCNTs composite solutions with various MWCNT concentrations (0 wt.%, 0.05 wt.%, 0.25 wt.% and 0.5 wt.%) were prepared. MWCNT loading is defined as the weight percentage of MWCNT with respect to total weight of the PVA/PEDOT:PSS/MWCNT composite solution. Since the higher loading of MWCNT results in severe agglomeration in the polymer matrix and poor interfacial adhesion between MWCNT and matrix, we prepared only composites with MWCNT concentrations up to 0.5 wt.%. Free standing films with a thickness of 20 $\mu$m were prepared by pouring this PVA/PEDOT:PSS/MWCNT solution into a petri dish, where it was kept at 40°C for 24 h to evaporate the solvent. Free standing films were peeled off manually and used for further characterization.

Neat PVA film was also prepared by the same method for comparison of EMI performance of the film with MWCNT filler in PVA/PEDOT:PSS. Figure 1a shows the chemical structure of PEDOT:PSS and PVA and Fig. 1b shows the schematic diagram of the preparation of PVA/PEDOT:PSS/MWCNT composite free-standing flexible film.

## CHARACTERIZATION

Electrical conductivity of the composite films was measured using a four-point probe technique with a Keithley 2400 source measure unit. Surface morphology of the composite films was observed using a Carl Zeiss supra 40 VP field emission scanning electron microscope (FESEM) at an accelerating voltage of 3 kV. Transmission electron microscopy (TEM) analysis was carried out using a Jeol/JEM 2100 microscope. X-ray diffraction (XRD) measurements were carried out using x-ray diffractometer (PANalytical X'PERT PRO) equipped with Cu K$_\alpha$ source ($\lambda$ = 1.5418 Å). The mechanical strength of the composite films was measured by a universal testing machine (UTM, Shimadzu, AGI 10kN), and test speed for griping surface is 50 mm/min;) as per ISO 527-2 1BB (International Organization for Standardization). EMI shielding performance of the composite flexible films was studied using a vector network analyzer (VNA) (Rohde & Schwarz ZVB 20) with X-band rectangular waveguide of dimensions 22.86 mm × 10.16 mm. The measurements were done by placing the composite films on the flanges of two standard X-band waveguides joined to coaxial waveguide adapters, which were connected to the ports of the VNA. Calibration of the VNA was done using the Through-Reflect-Line (TRL) method before employing the rectangular sample holder with samples for the measurements.

## RESULTS AND DISCUSSION

### Structural and Morphological Properties

Figure 2a shows the FESEM image of the PVA/PEDOT:PSS film. The FESEM images of PVA/PEDOT:PSS/MWCNT composite films with various MWCNT loadings are shown in Fig. (2b, c, and d). PEDOT:PSS coated-MWCNTs are distributed uniformly over the polymer matrix. As MWCNT loading increases, it is observed that highly conducting pathways are formed through the host PVA matrix and at higher CNT loading (0.5 wt.%); the MWCNT interconnected networks are also increased. The
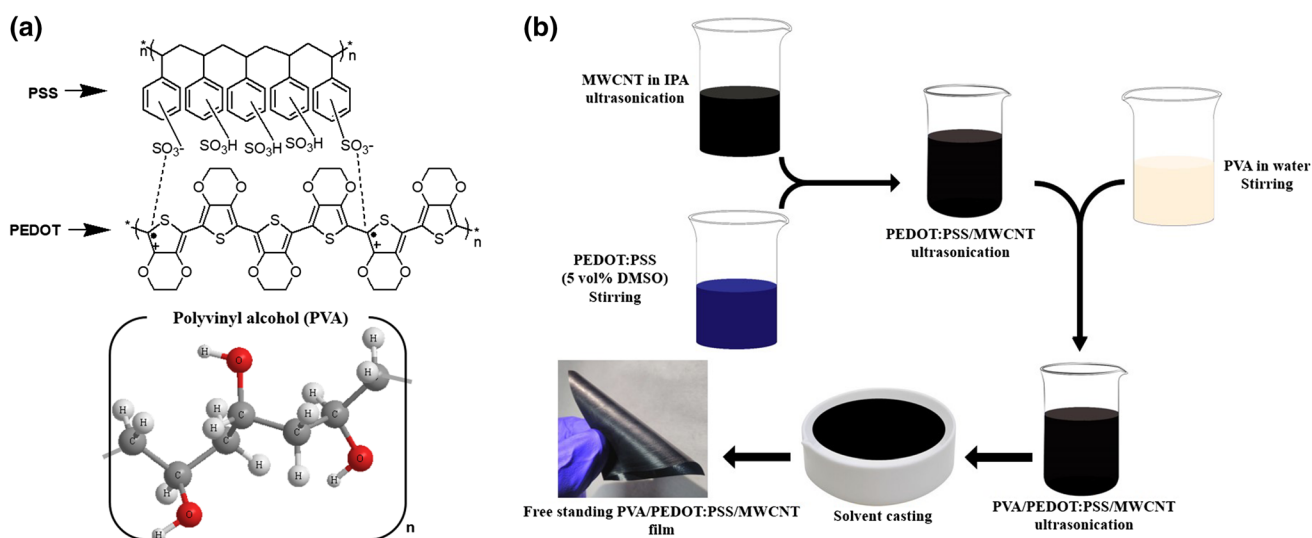
Fig. 1. (a) Chemical structure of PEDOT:PSS and PVA; (b) schematic representation of the preparation of PVA/PEDOT:PSS/MWCNT free-standing film.
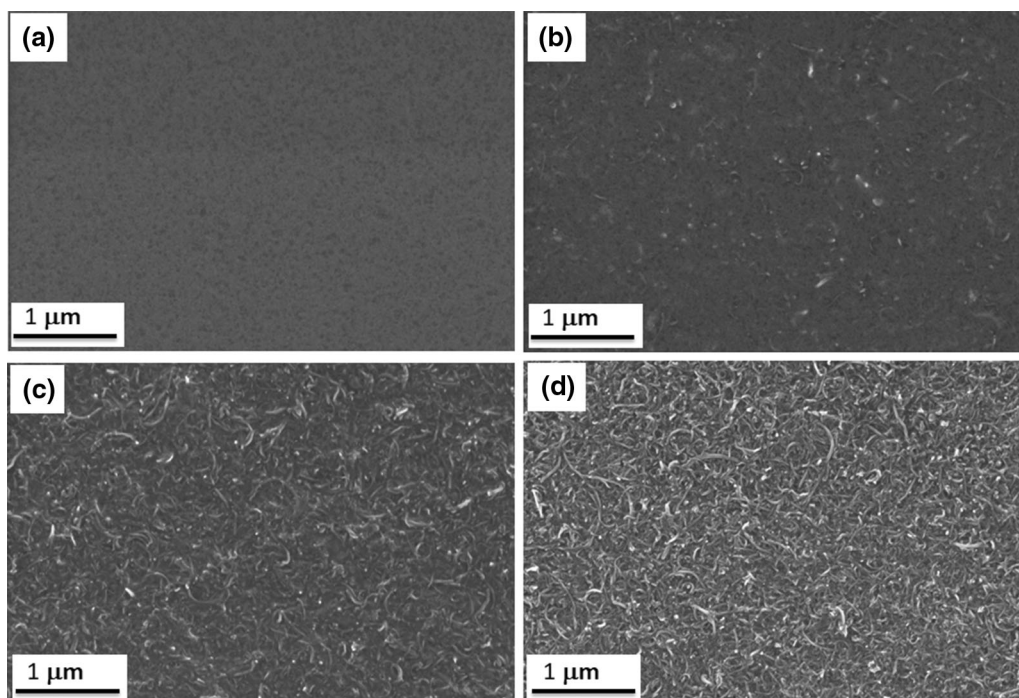


Fig. 2. FESEM images of (a) PVA/PEDOT:PSS film, PVA/PEDOT:PSS/MWCNT composite films with (b) 0.05 wt.%, (c) 0.25 wt.% (d) 0.5 wt.% of MWCNT.

high aspect ratio of MWCNTs facilitates percolating paths at a very low volume fraction. Also, the interconnected networks of PEDOT:PSS coated MWCNTs in the PVA matrix can be very well observed in the TEM images (Fig. 3a and b). In PVA/PEDOT:PSS/MWCNT films, interaction between the MWCNTs increases as MWCNT loading increases from 0 wt.% to 0.5 wt.%. These interconnected MWCNT networks in the PVA polymer matrix increase the overall mechanical strength of

the composite film. XRD patterns of PVA and PVA/PEDOT:PSS/MWCNT with MWCNT loading from 0 wt.% to 0.5wt.%, respectively, are shown in the Fig. 4. PVA is a semi crystalline polymer that has a diffraction peak at $2\theta = 19.5°$, which corresponds to the (101) plane. In PVA/PEDOT:PSS/MWCNT composite films, a characteristic peak of MWCNT at $2\theta = 25.9°$ corresponding to the (002) plane is observed. In the composite films, the intensity of the MWCNT diffraction peak corresponding to the
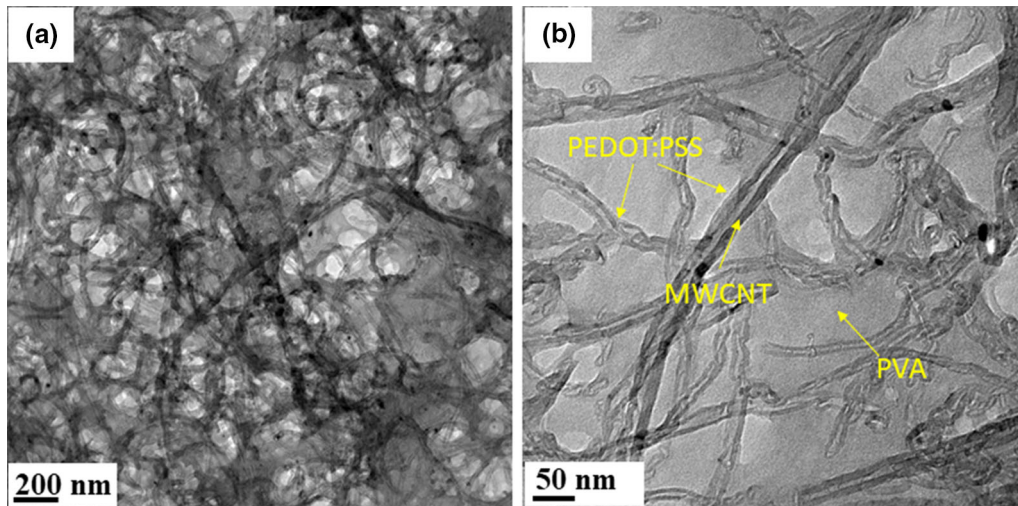
Fig. 3. (a) TEM images of PVA/PEDOT:PSS/MWCNT composite with 0.5 wt.% of MWCNT and (b) magnified view of the same composite film.
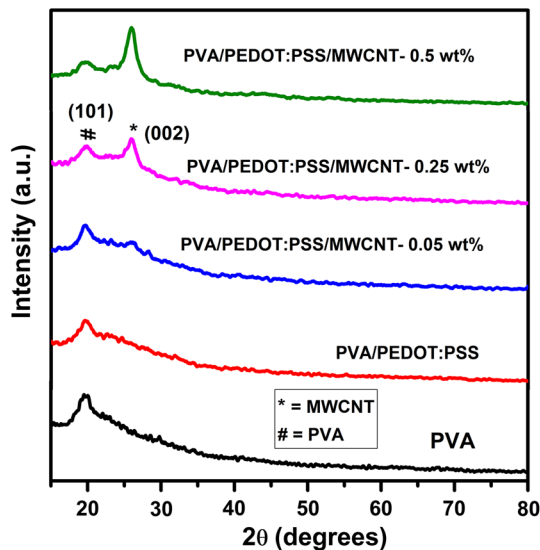


Fig. 4. XRD patterns of PVA, PVA/PEDOT:PSS, and its composite films.



Fig. 5. WAXRD pattern of PVA/PEDOT:PSS/MWCNT composite films with 0.5 wt.% of MWCNT; the inset shows a magnified view of WAXRD pattern.

(002) plane is increased due to an increase of MWCNT loading. Detailed characteristics of the composite film with 0.5 wt.% of MWCNT were observed by wide angle XRD (WAXRD), as shown in Fig. 5, and more peaks of PVA and MWCNT were observed. The peak at $2\theta = 40.8°$ shows the amorphous phase of the PVA, and peaks at $2\theta$ of $43°$ and $53.5°$ corresponds to the MWCNT.

## Electrical Conductivity Measurement

The electrical conductivities of PVA/PEDOT:PSS and PVA/PEDOT:PSS/MWCNT composite films with various MWCNT loadings were analyzed by four probe method, and are shown in Fig. 6a. Even though PEDOT is a highly conducting polymer due to its π-conjugated chain, it is not water soluble.
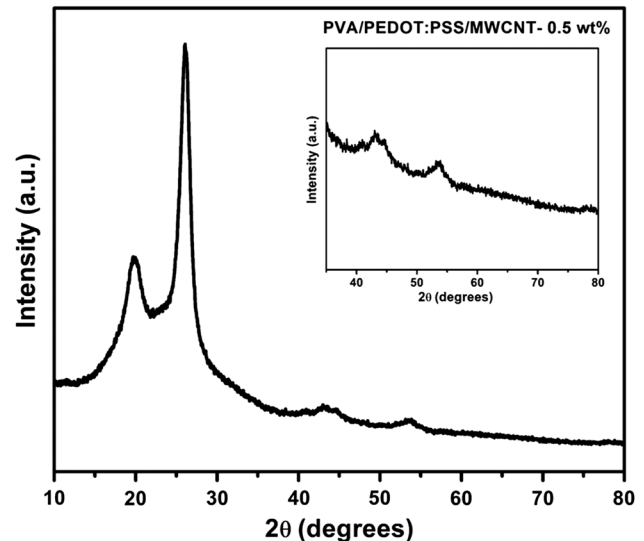
Usually, water-soluble electrolyte PSS is added to improve the water solubility of PEDOT. The electrical conductivity of pristine PEDOT:PSS is low (∼ 1 S/cm) due to the insulating polymer PSS. It consists of a conductive PEDOT-rich core embedded within the PSS insulating polymer (Fig. 6c). The insulating polymer blocks the charge carrier transport within the polymer and separates the PEDOT grains from each other. By introducing an organic solvent like DMSO, as shown in Fig. 6c, the insulating PSS barrier can be removed, thereby increasing the average distance between the conductive PEDOT grains; i.e. the PEDOT chains rearrange themselves and make charge transport easier. DMSO interacts with the sulfonic acid group of PSS polymer and separates it by weakening the

Facile Preparation of Lightweight and Flexible PVA/PEDOT:PSS/MWCNT Ternary Composite
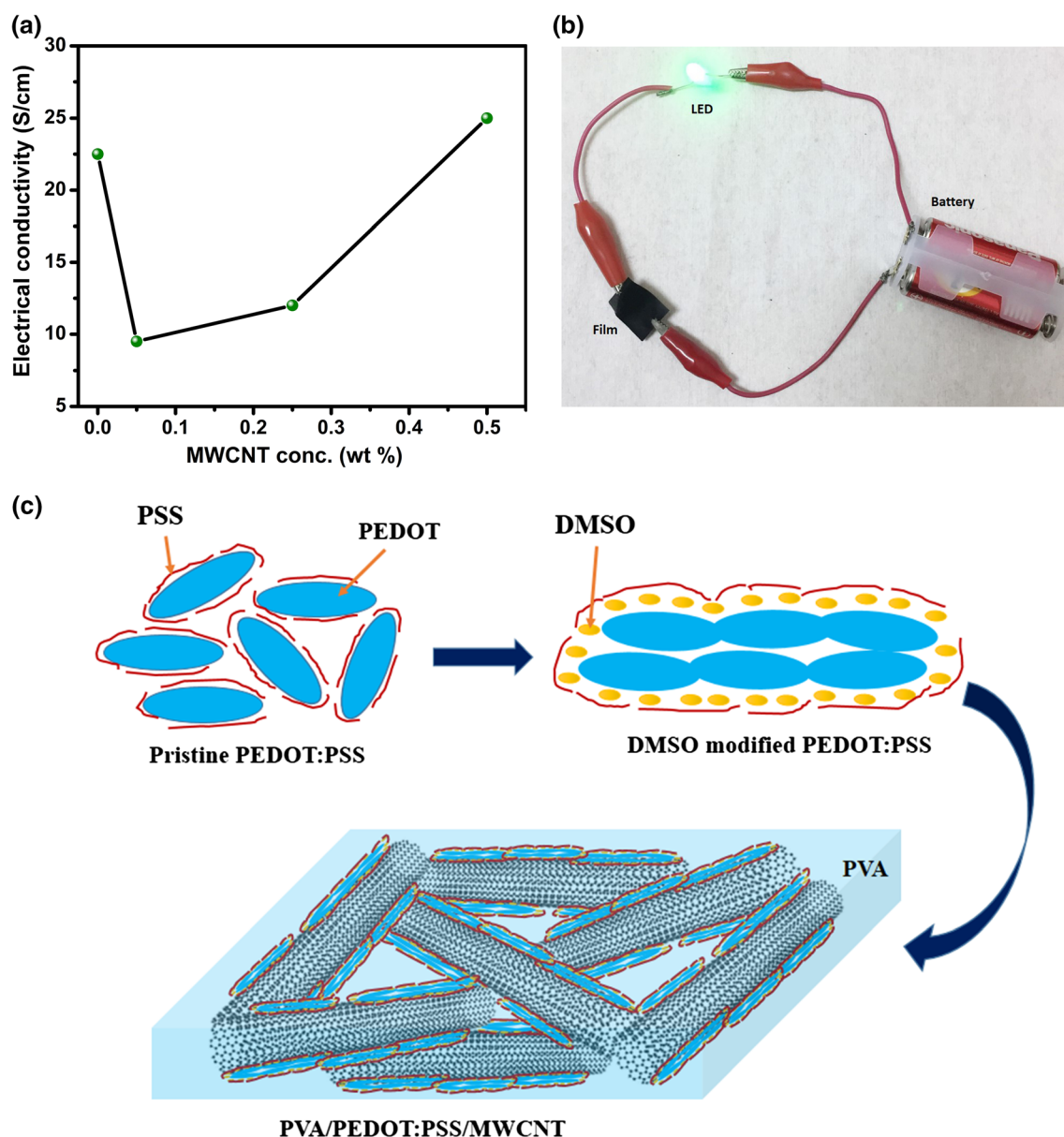for High-Performance EMI Shielding in the X-Band Through Absorption Mechanism

1695



Fig. 6. Electrical conductivity of (a) the PVA/PEDOT:PSS and PVA/PEDOT:PSS/MWCNT composite films with various MWCNT loading; (b) digital image that shows the electrical conductivity with PVA/PEDOT:PSS/MWCNT composite film in a circuit. (c) Schematic conformation of PEDOT:PSS after mixing with DMSO and formation of PVA/PEDOT:PSS/MWCNT composite film.

Coulomb attraction between PEDOT and PSS. As a result, PEDOT polymer chains rearrange themselves, leading to an increase in the inter-chain interaction and enhancement in conductivity. Electrical conductivity of DMSO-modified PEDOT:PSS was ∼ 200 S/cm. PVA/PEDOT:PSS showed an electrical conductivity of 22.5 S/cm. This reduction in electrical conductivity is due to the presence of insulating PVA polymer matrix. Electrical conductivity of the PVA/PEDOT:PSS/MWCNT composite films increases as a function of MWCNT concentration. In the PVA/PEDOT:PSS/MWCNT composite, PEDOT:PSS coated over the MWCNT makes excellent conducting networks within the PVA matrix. The presence of PEDOT:PSS significantly contributes to the enhancement in conductivity of composite film, and hence limits the usage of high amounts of MWCNT. This small dosage of MWCNT loading prevents the aggregation of MWCNT in the composite films. At a loading of 0.05 wt.% of MWCNT, the conductivity of PVA/PEDOT:PSS/MWCNT composite film decreased from 22.5 S/cm to 9.5 S/cm. Further, electrical conductivity is increased as a function of MWCNT concentration due to the increase in MWCNT conductive pathways throughout the polymer matrix. Figure 6b is a photograph with the composite film in the electrical circuit demonstrating the electrical conductivity of the free-standing composite film prepared with an MWCNT wt.% of 0.5.

The mechanical features of nanocomposite films are controlled by their hierarchical structure. Therefore, distribution of nanofillers, nature of the polymer, percolation threshold and interfacial interaction between filler and polymer matrix are the key factors that determine the mechanical properties in a composite or multi-component system. Figure 7 shows stress–strain curves of the PVA, PVA/PEDOT:PSS, and PVA/PEDOT:PSS/MWCNT composite films with various MWCNT loadings. The strengthening effect of the MWCNTs in composite films was evaluated by measuring tensile strength at room temperature. Variation of Young's modulus, tensile strength, and elongation at break for different composite films are shown in Fig. 8a, b, and c. Pure PVA shows a high elongation at break of 338.7%, a low Young's modulus of 95 MPa, and tensile strength of 39.1 MPa as compared to composite films. For PVA/PEDOT:PSS composite film, in the absence of MWCNT, Young's modulus rapidly increases to 369.1 MPa, tensile strength increases to 48.4 MPa, and elongation at break decreases to $\sim 181\%$. This is attributed to the presence of PEDOT:PSS within the PVA matrix. At the MWCNT loading of 0.05 wt.%, a slight increment in Young's modulus is observed, while tensile strength does not vary significantly. But, as the MWCNT concentration increases from 0.25 wt.% to 0.5 wt.%, a significant increment in Young's modulus and tensile strength is observed. This is mainly due to the interconnected MWCNT network, which provides better stress transfer under tensile loading and makes the composite film stronger. But elongation at break is considerably reduced due to the addition of MWCNTs, which act as stress concentrators. Results suggests that as the MWCNT concentration increases, interaction between the MWCNTs begins to dominate, and consequently tensile strength and Young's modulus increases. For 0.5 wt.% of MWCNT composite films, Young's modulus of 1723 MPa and tensile strength of

$\sim 134$ MPa is observed. This indicates that the PEDOT:PSS-coated MWCNTs networks facilitate efficient stress transfer within the polymer matrix. This is further confirmed from the TEM images and tensile measurements indicating that the MWCNTs network is well localized within the polymer matrix.

## Magnetic Properties of Composite Films

Magnetic properties of the PVA/PEDOT:PSS/MWCNT composite films were explained using the *M–H* curve (Fig. 9a and b) composites measured at room temperature using a vibrating sample magnetometer (VSM). PVA/PEDOT:PSS films show diamagnetic response. PVA/PEDOT:PSS/MWCNT composite films show ferromagnetic behavior with diamagnetic background. As MWCNT increases, saturation magnetization is increased with no significant change in the hysteresis loop. For the film with 0.25 wt.% of MWCNT, coercivity (Hc), remanent magnetization (Mr), saturation magnetic field (Ms) and squareness ratio (Mr/Ms) were found to be 56.6 Oe, 0.028 emu/cm$^3$, 0.199 emu/cm$^3$ and 0.14, respectively. Coercivity (Hc), remanent magnetization (Mr), saturation magnetic field (Ms) and squareness ratio (Mr/Ms) for the films with 0.5 wt.% of MWCNT were found to be 54 Oe, 0.038 emu/cm$^3$, 0.496 emu/cm$^3$, and 0.07, respectively. Ferromagnetic behavior in the films is mainly due to hydrogen chemisorption defects created during the acid-purification process.[45] Remaining catalyst particles in acid treated MWCNT also slightly affects magnetization of the films.[46]

## EMI Shielding Performance of PVA/PEDOT:PSS/MWCNT Composite Film

Electromagnetic interference shielding can be expressed in terms of shielding effectiveness (SE), which is the logarithmic ratio of the transmitted to the incident electric (or magnetic) field powers of electromagnetic waves and is usually measured in decibels (dB).

$$\mathrm{SE} = 10 \log \frac{P_i}{P_0} \qquad (1)$$

In practical applications, EMI shielding materials should exhibit EMI SE $\sim 20$ dB which allows only 1% of the electromagnetic waves to be transmitted.[6] The scattering parameters ($S_{11}$ or $S_{22}$ and $S_{12}$ or $S_{21}$) were measured and are related to the reflected and transmitted power. When microwave radiation is incident on shielding materials, the sum of transmitted ($T$), reflected ($R$) and absorbed ($A$) radiations must be equal to one. $T$, $R$ and $A$ can be obtained from the measured scattering parameters using the equation, $T = |S_{12}|^2 = |S_{21}|^2$, $R = |S_{11}|^2 = |S_{22}|^2$ and $A = 1 - R - T$, respectively. Absorption is due to the presence of both electric and magnetic dipoles in the material. Reflection occurs when
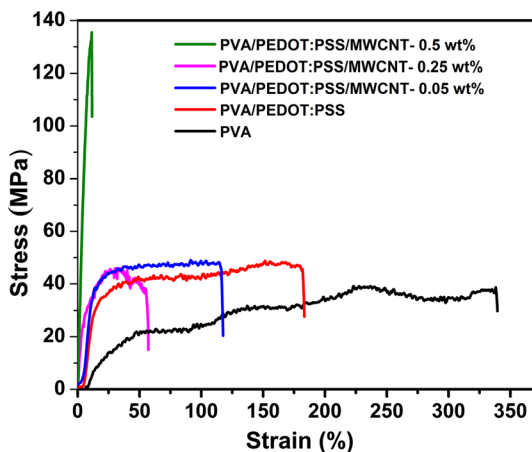


Fig. 7. Stress–strain curves of a neat PVA, PVA/PEDOT:PSS and PVA/PEDOT:PSS/MWCNT composite films with different MWCNT concentrations.
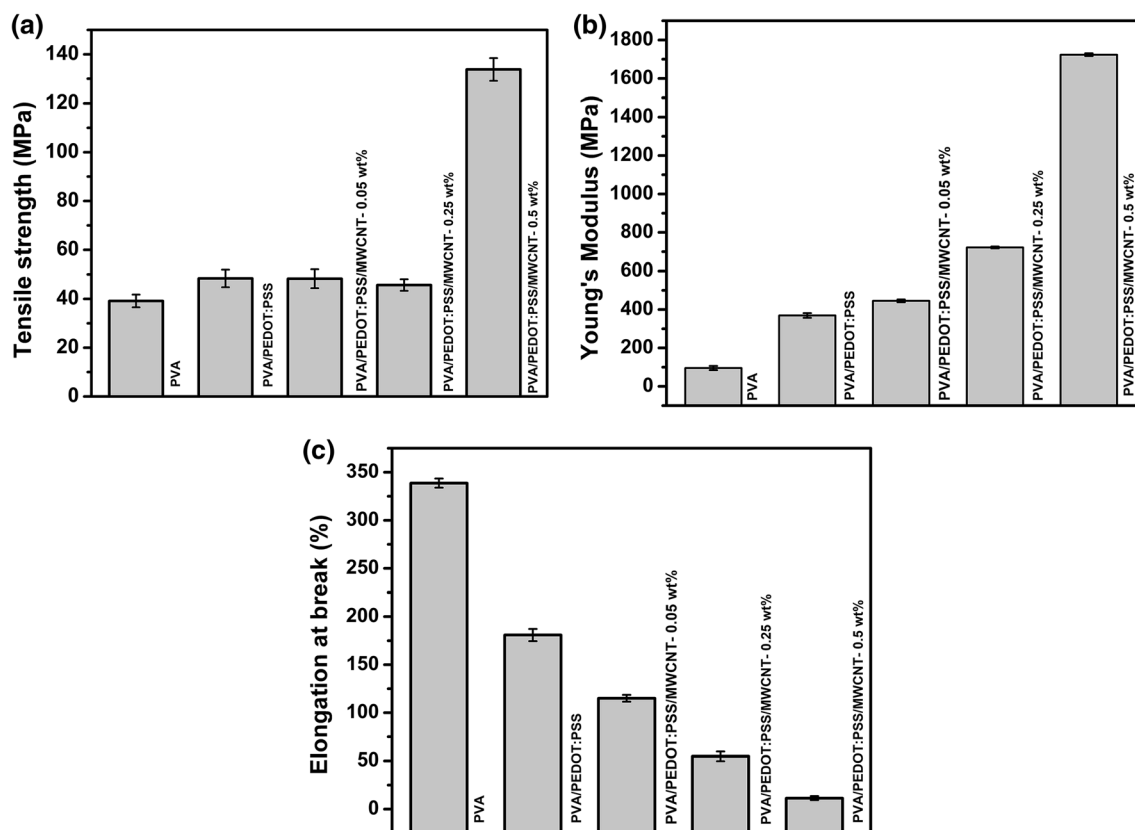
Fig. 8. (a) Tensile strength, (b) Young's modulus and (c) elongation at break of a pure PVA, PVA/PEDOT:PSS and PVA/PEDOT:PSS/MWCNT composite films with different MWCNT loading.
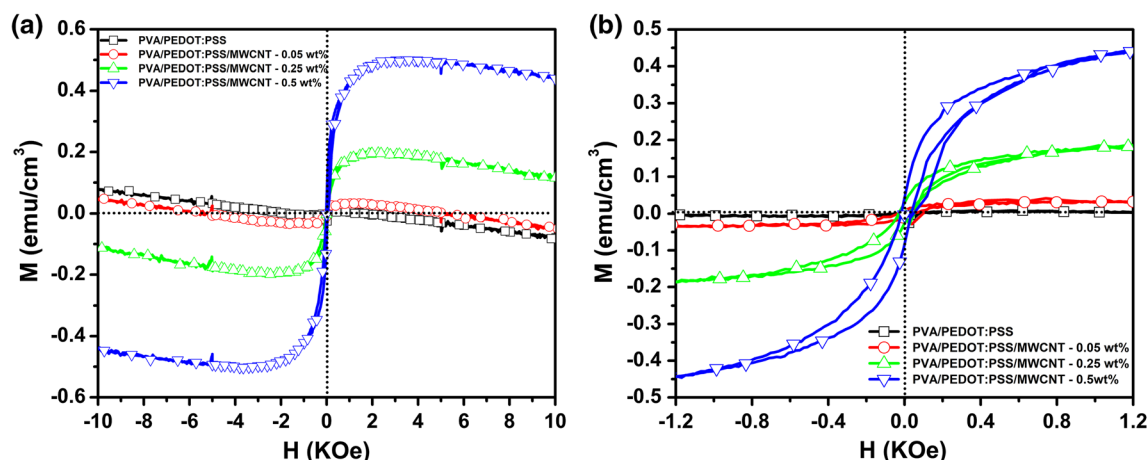


Fig. 9. (a) Magnetization (*M*) versus applied field (*H*) measured at 300 K for PVA/PEDOT:PSS and PVA/PEDOT:PSS/MWCNT with various concentration of MWCNT and (b) its magnified view.

materials have high electrical conductivity and mobile charge carriers, which interact with the incident EM waves. Multiple reflections occur when EM waves scatter due to the inhomogeneity in the material. Total shielding effectiveness ($SE_T$) is the contribution from reflection, absorption and multiple reflections of electromagnetic radiations. Hence,

$$SE_T = SE_A + SE_R + SE_M \qquad (2)$$

$SE_A$, $SE_R$ and $SE_M$ are the shielding effectiveness by absorption, reflection and multiple reflection, respectively. If $SE_T$ is greater than 15 dB, $SE_M$ can be neglected[37] and hence, $SE_T$ is assumed to be

$$SE_T = SE_A + SE_R \qquad (3)$$

$SE_R$ and $SE_A$ can be calculated from scattering parameters using the equations

$$SE_R = 10 \log \left( \frac{1}{1 - |S_{11}|^2} \right) \quad (4)$$

$$SE_A = 10 \log \left( \frac{1 - |S_{11}|^2}{|S_{21}|^2} \right), \quad (5)$$

so the total shielding effectiveness ($SE_T$) is given by the equation

$$SE_T = 10 \log \left( \frac{1}{|S_{21}|^2} \right). \quad (6)$$

To analyze the EMI shielding performance of the PVA/PEDOT:PSS/MWCNT composite film of thickness 20 $\mu m$, scattering parameters were measured ($S_{11}$ and $S_{21}$) using a vector network analyzer via waveguide method over the frequency range (8–12 GHz). EMI SE of the neat PVA and the composite films are given in the Fig. 10. The neat PVA was almost transparent to the EM waves, and its EMI SE is nearly 0 dB due to its insulating nature. An obvious EMI shielding effect could be observed due to the incorporation of DMSO-modified PEDOT:PSS in PVA. PVA/PEDOT:PSS shows an EMI SE of 52.5 dB at 9 GHz. This value is high enough for practical application, which means that only 0.0006% of the EM waves could be transmitted through the PVA/PEDOT:PSS composite film. EMI SE is increased by adding MWCNT into the PVA/PEDOT:PSS composite.

At a loading of 0.05 wt.% of MWCNT, composite films showed a slight decrease in EMI SE from 52.5 dB to 44.5 dB due to the decrease in electrical conductivity of the film. However, further increase in the MWCNT loading (0.25 wt.%), increased the EMI SE to ~ 50 dB. At a loading of 0.5 wt.% of MWCNT in composite film, the highest EMI SE around 60.3 dB is obtained which is the highest value among the carbon nanotube-based composite
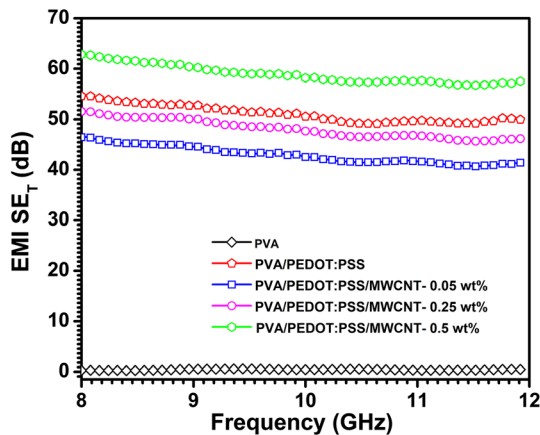


Fig. 10. Frequency dependence of total EMI SE of neat PVA and PVA/PEDOT:PSS/MWCNT composite films at different MWCNT loadings.

flexible, free-standing thin films. An EMI SE around 62 dB has been reported for PEDOT:PSS/WPU composite film having a PEDOT to PSS ratio of 0.4 and a film thickness of 0.15 mm.[31] Nevertheless, the composite film fabricated in the present work is certainly superior, due to the fact that the $SE_T$ of 60 dB was achieved for a film thickness of just 20 microns and PEDOT to PSS ratio of 0.625. As described earlier, the possible mechanism behind the attenuation of EM waves is absorption and/or reflection of the EM waves by EMI shielding material. Hence, understanding the mechanism of EMI shielding is very essential. $SE_R$ and $SE_A$ of composite films with different weight percentage of MWCNT (0 wt.%, 0.05 wt.%, 0.25 wt.% and 0.5 wt.%) in the X-band region were calculated using Eqs. 4 and 5, and the sum of $SE_R$ and $SE_A$ gives $SE_T$ , as shown in Fig. 11a, b, c, and d. Figure 11e shows the variation of average $SE_A$, $SE_R$ and $SE_T$ of the composite films as a function of MWCNT loading. In all cases, $SE_A$ is higher than that of $SE_R$ for all composite films. As MWCNT concentrations increase from 0 wt.% to 0.5 wt.%, $SE_A$ increases, while $SE_R$ is almost constant. $SE_R$ of PVA/PEDOT:PSS film is slightly higher than that of composite film at 0.05 wt.% MWCNT loading, due to the increased electrical conductivity.

The remarkable increase in $SE_A$ is explained by the wave absorbing mechanism of CNT due to its chiral structures and quanta size. The splitting of energy levels of electrons occurs due to the quanta size effect and the corresponding energy gap matches the microwave energy level, which leads to the enhanced absorption of electromagnetic waves.[47] From the present study, it is apparent that absorption is the dominant mechanism in PVA/PEDOT:PSS and PVA/PEDOT:PSS/MWCNT composite films. Shielding effectiveness due to absorption is due to the presence of conductive networks, which makes more surface area available for interaction with incoming EM waves. Moreover, in the PVA/PEDOT:PSS/MWCNT composite films, a better conductive path is formed due to the entanglement of PEDOT:PSS coated MWCNTs. This conducting path can induce charge transport, and thereby EM waves are attenuated by conduction loss; i.e. incoming EM waves cannot transmit through the film very easily due to the conducting networks. Moreover, in PVA/PEDO:PSS/MWCNT with 0.25 wt.% and 0.5 wt.% of MWCNT, shielding can also be attributed to electromagnetic absorption due to the existence of magnetic dipoles in MWCNT, which thereby improves radiation absorption more than radiation reflection. The absorption mechanism can be understood in detail by calculating skin depth using measured scattering parameters. $SE_R$ and $SE_A$ can be related to various parameters like skin depth ($\delta$), film thickness ($d$), electrical conductivity ($\sigma$), wave frequency ($f$), magnetic permeability ($\mu$), and impedance in free space ($\eta_0$) by the following theoretical formula.[21]

Facile Preparation of Lightweight and Flexible PVA/PEDOT:PSS/MWCNT Ternary Composite
for High-Performance EMI Shielding in the X-Band Through Absorption Mechanism
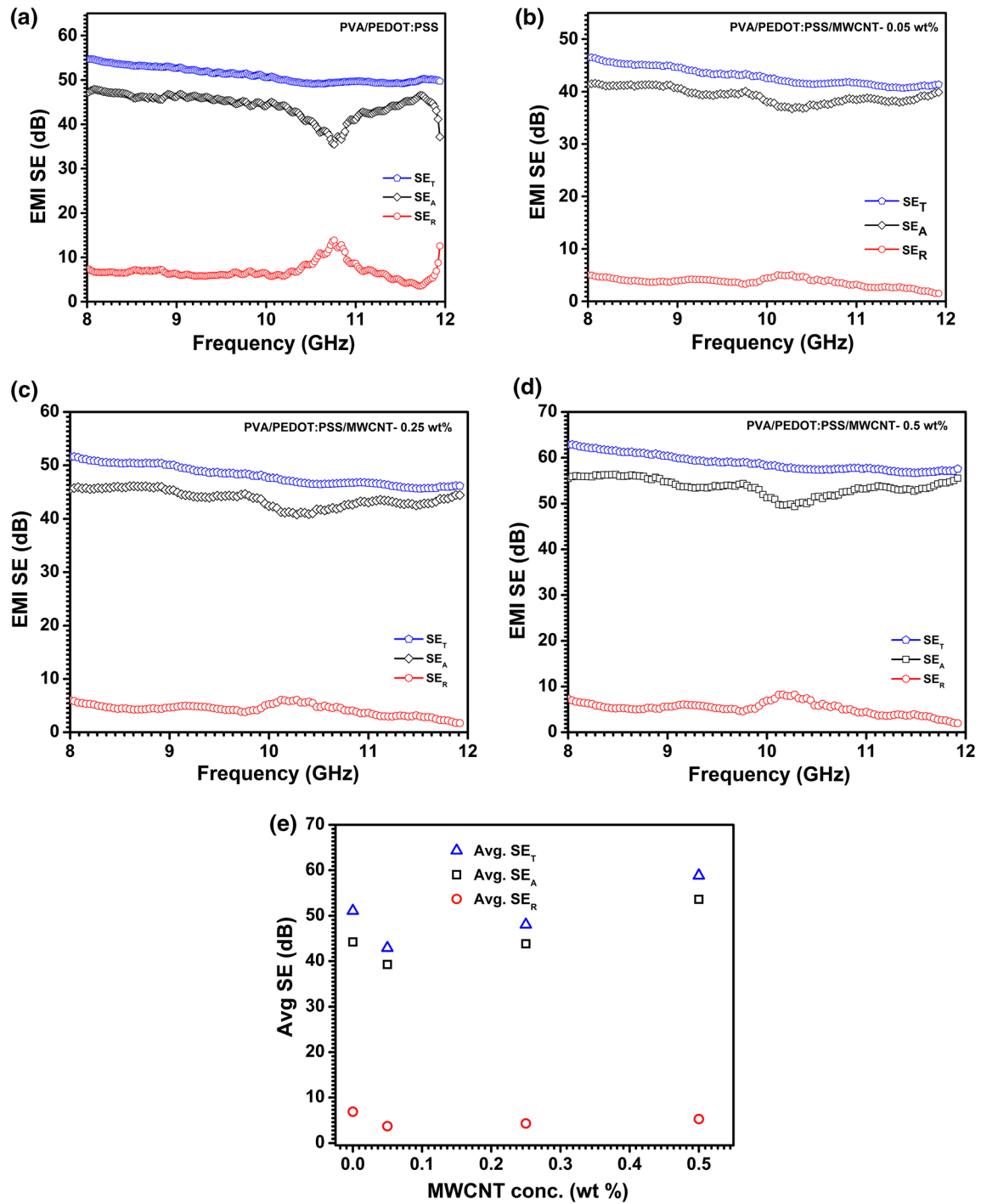
1699



Fig. 11. EMI $SE_A$, $SE_R$ and $SE_T$ of (a) PVA/PEDOT:PSS and PVA/PEDOT:PSS/MWCNT films at a MWCNT loading of (b) 0.05 wt.%, (c) 0.25 wt.% and (d) 0.5 wt.%; (e) average $SE_A$, $SE_R$ and $SE_T$ of composite films as a function of MWCNT loading.

$$SE_R = 20 \log\left(\frac{\eta_0}{4}\sqrt{\frac{\sigma}{2\pi f \mu}}\right) \qquad (7)$$

$$\delta = \sqrt{\frac{1}{\pi f \mu \sigma}} \qquad (8)$$

$$SE_A = 8.68\frac{d}{\delta} \qquad (9)$$

From Eqs. (7 and 8), it is clearly seen that, as electrical conductivity increases, $SE_R$ increases, whereas the skin depth decreases. Also, the skin depth decreases as $SE_A$ increases. In the composite
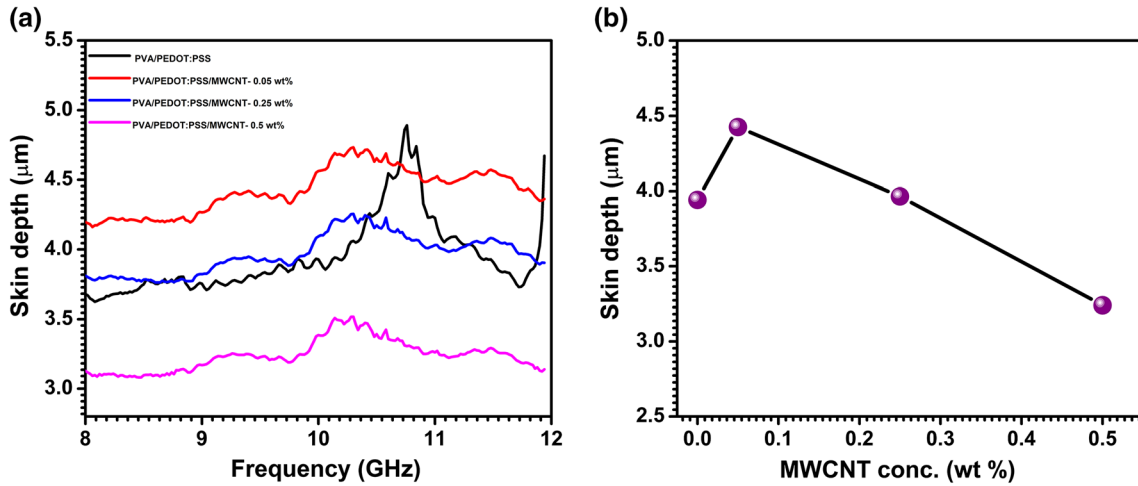
Fig. 12. (a) Variation of skin depth with the frequency of various MWCNT loading (b) plot of skin depth versus with different MWCNT concentration.

**Table II. Electrical conductivity, elongation at break, Young's modulus and shielding effectiveness of PVA/PEDOT:PSS/MWCNT composite films**

| Sample name | Conductivity (S/cm) | Elongation at break (%) | Young's modulus (MPa) | Shielding effectiveness at 9 GHz (SE) dB |
|---|---|---|---|---|
| Neat PVA | – | 338.74 | 95 | 0.49 |
| PVA/PEDOT:PSS | 22.5 | 180.86 | 369 | 52.58 |
| PVA/PEDOT:PSS/MWCNT 0.05 wt.% | 9.5 | 114.99 | 445 | 44.59 |
| PVA/PEDOT:PSS/MWCNT 0.25 wt.% | 12 | 54.72 | 721 | 50.05 |
| PVA/PEDOT:PSS/MWCNT 0.5 wt.% | 25 | 11.32 | 1723 | 60.37 |

films, $SE_R$ maintained an insignificant change at a fluctuation of 3.6–5.2 dB by the added MWCNTs, while $SE_A$ increased as a function of MWCNT loading. From this observation, it is clear that the $SE_A$ contribution to the total SE is more than 90%, while the $SE_R$ contribution is very limited. $SE_A$ and electrical conductivity are inversely proportional to skin depth. The variation of skin depth of the composite films with different MWCNT loadings as a function of frequency is shown in Fig. 12a. Figure 12b shows the variation of average skin depth with respect to MWCNT loading. This decrease in skin depth is due to the high aspect ratio of the MWCNTs. In addition, it is also observed that the total SE of the films increases with respect to MWCNT loading. The electrical conductivity, elongation at break, Young's modulus and SE at 9 GHz of the composite films are summarized in Table II.

Overall, the prepared composite film was capable of absorbing the incoming electromagnetic radiation. This study clearly proved that this simple method has led to concurrent improvement in electrical, mechanical and EMI shielding properties. This solution method also shows that the flexibility (Fig. 1b) and lightweight of the composite film can

be retained and excellent EMI shielding performance can be obtained by tailoring the composite with the incorporation of MWCNTs.

**CONCLUSIONS**

Highly conducting free-standing, flexible and lightweight composite films with excellent electromagnetic shielding capability in the X-band region (8–12 GHz) were fabricated using a simple solvent casting method. DMSO modified PEDOT:PSS was used for the fabrication of the composite film. PVA/PEDOT:PSS/MWCNT composite films with different MWCNT loadings (0–0.5 wt.%) were prepared. Incorporation of MWCNT increases the overall mechanical strength of the composite films by acting as stress concentrators. The composite films with 0.5 wt.% of MWCNT loading possessed superior EMI shielding effectiveness of $\sim 60$ dB with considerable tensile strength at a thickness of 20 $\mu$m. DMSO modification of PEDOT:PSS can simultaneously improve the electrical conductivity and reduce usage of high MWCNT loading for conductivity enhancement. The MWCNTs in the composite film facilitate better stress transfer under tensile

Facile Preparation of Lightweight and Flexible PVA/PEDOT:PSS/MWCNT Ternary Composite
for High-Performance EMI Shielding in the X-Band Through Absorption Mechanism

1701

loading. The PVA/PEDOT:PSS/MWCNT free-standing composite films shielded EM radiation mostly by an absorption mechanism. This study signifies that this simple strategy, based on flexible, free-standing, thin and lightweight PEDOT:PSS–MWCNT composite film, can be used as high-efficiency electromagnetic screening devices for next-generation flexible electronic devices.

## ACKNOWLEDGMENTS

## CONFLICT OF INTEREST

The authors declare that they have no conflict of interest.

## REFERENCES

1. M. Hu, J. Gao, Y. Dong, K. Li, G. Shan, S. Yang, and R.K.Y. Li, *Langmuir* 28, 7101 (2012).
2. D.X. Yan, H. Pang, B. Li, R. Vajtai, L. Xu, P.G. Ren, J.H. Wang, and Z.M. Li, *Adv. Funct. Mater.* 25, 559 (2015).
3. M. Layani, A. Kamyshny, and S. Magdassi, *Nanoscale* 6, 5581 (2014).
4. D. Markham, *Mater. Des.* 21, 45 (1999).
5. C.J. von Klemperer and D. Maharaj, *Compos. Struct.* 91, 467 (2009).
6. D.D.L. Chung, *Carbon* 50, 3342 (2012).
7. T. Ramanathan, A.A. Abdala, S. Stankovich, D.A. Dikin, M. Herrera-Alonso, R.D. Piner, D.H. Adamson, H.C. Schniepp, X. Chen, R.S. Ruoff, S.T. Nguyen, I.A. Aksay, R.K. Prud'-Homme, and L.C. Brinson, *Nat. Nanotechnol.* 3, 327 (2008).
8. D.D.L. Chung, *J. Mater. Eng. Perform.* 9, 350 (2000).
9. I. C. P. Project, *An Introduction to Conductive Polymer Composites* (Akron: Smithers Rapra Technology, 2011).
10. S.P. Pawar, S. Kumar, A. Misra, S. Deshmukh, K. Chatterjee, and S. Bose, *RSC Adv.* 5, 17716 (2015).
11. S.P. Pawar, D.A. Marathe, K. Pattabhi, and S. Bose, *J. Mater. Chem. A* 3, 656 (2015).
12. S.P. Pawar, S. Stephen, S. Bose, and V. Mittal, *Phys. Chem. Chem. Phys.* 17, 14922 (2015).
13. G.P. Kar, S. Biswas, and S. Bose, *Phys. Chem. Chem. Phys.* 17, 14856 (2015).
14. P. Xavier and S. Bose, *Phys. Chem. Chem. Phys.* 17, 14972 (2015).
15. S. Biswas, *Phys. Chem. Chem. Phys.* 17, 27698 (2015).
16. S. Biswas, G.P. Kar, and S. Bose, *Nanoscale* 7, 11334 (2015).
17. M. Sharma, G. Madras, and S. Bose, *J. Mater. Chem. A* 3, 5991 (2015).
18. V. Bhingardive, M. Sharma, S. Suwas, G. Madras, and S. Bose, *RSC Adv.* 5, 35909 (2015).
19. S. Biswas, S.S. Panja, and S. Bose, *Mater. Chem. Front.* 1, 132 (2017).
20. Y. Wu, Z. Wang, X. Liu, X. Shen, Q. Zheng, Q. Xue, and J.K. Kim, *ACS Appl. Mater. Interfaces* 9, 9059 (2017).
21. Y. Xu, Y. Li, W. Hua, A. Zhang, and J. Bao, *ACS Appl. Mater. Interfaces* 8, 24131 (2016).
22. B. Shen, Y. Li, W. Zhai, and W. Zheng, *ACS Appl. Mater. Interfaces* 8, 8050 (2016).
23. T.M. Swager, *Macromolecules* 50, 4867 (2017).
24. S.T. Hsiao, C.C.M. Ma, W.H. Liao, Y.S. Wang, S.M. Li, Y.C. Huang, R. Bin Yang, and W.F. Liang, *ACS Appl. Mater. Interfaces* 6, 10667 (2014).
25. W.L. Song, J. Wang, L.Z. Fan, Y. Li, C.Y. Wang, and M.S. Cao, *ACS Appl. Mater. Interfaces* 6, 10516 (2014).
26. A. Chaudhary, S. Kumari, R. Kumar, S. Teotia, B.P. Singh, A.P. Singh, S.K. Dhawan, and S.R. Dhakate, *ACS Appl. Mater. Interfaces* 8, 10600 (2016).
27. B. Zhao, C. Zhao, R. Li, S.M. Hamidinejad, and C.B. Park, *ACS Appl. Mater. Interfaces* 9, 20873 (2017).
28. H. Li, X. Lu, D. Yuan, J. Sun, F. Erden, F. Wang, and C. He, *J. Mater. Chem. C* 5, 8694 (2017).
29. S.M.N. Sultana, S.P. Pawar, M. Kamkar, and U. Sundararaj, J. Electron. Mater. (2019). https://doi.org/10.1007/s11664-019-07371-8.
30. H. Nallabothula, Y. Bhattacharjee, L. Samantara, and S. Bose, *ACS Omega* 4, 1781 (2019).
31. P. Li, D. Du, L. Guo, Y. Guo, and J. Ouyang, *J. Mater. Chem. C* 4, 6525 (2016).
32. M.L. Hallensleben, R. Fuss, and F. Mummy, in *Ullmann's Encyclopedia of Industrial Chemistry*, ed. B. Elvers (Wiley, Weinheim, 2000), pp. 1–23.
33. K. Lakshmi, H. John, K.T. Mathew, R. Joseph, and K.E. George, *Acta Mater.* 57, 371 (2009).
34. N. Muthukumar, G. Thilagavathi, and T. Kannaian, *High Perform. Polym.* 27, 105 (2015).
35. N. Joseph, C. Janardhanan, and M.T. Sebastian, *Compos. Sci. Technol.* 101, 139 (2014).
36. M. Chen, L. Zhang, S. Duan, S. Jing, H. Jiang, M. Luo, and C. Li, *Nanoscale* 6, 3796 (2014).
37. T.K. Gupta, B.P. Singh, S. Teotia, V. Katyal, S.R. Dhakate, and R.B. Mathur, *J. Polym. Res.* 20, 32 (2013).
38. T.K. Gupta, B.P. Singh, S.R. Dhakate, V.N. Singh, and R.B. Mathur, *J. Mater. Chem. A* 1, 9138 (2013).
39. J. Ling, W. Zhai, W. Feng, B. Shen, J. Zhang, and W.G. Zheng, *ACS Appl. Mater. Interfaces* 5, 2677 (2013).
40. Z. Chen, C. Xu, C. Ma, W. Ren, and H.M. Cheng, *Adv. Mater.* 25, 1296 (2013).
41. Z. Zeng, M. Chen, Y. Pei, S.I. Seyed Shahabadi, B. Che, P. Wang, and X. Lu, *ACS Appl. Mater. Interfaces* 9, 32211 (2017).
42. S.-T. Hsiao, C.-C.M. Ma, H.-W. Tien, W.-H. Liao, Y.-S. Wang, S.-M. Li, and Y.-C. Huang, *Carbon* 60, 57 (2013).
43. S.K. Marka, B. Sindam, K.C. James Raju, and V.V.S.S. Srikanth, *RSC Adv.* 5, 36498 (2015).
44. S.T. Hsiao, C.C.M. Ma, H.W. Tien, W.H. Liao, Y.S. Wang, S.M. Li, C.Y. Yang, S.C. Lin, and R. Bin Yang, *ACS Appl. Mater. Interfaces* 7, 2817 (2015).
45. D.C. Yan, S.Y. Chen, M.K. Wu, C.C. Chi, J.H. Chao, and M.L.H. Green, *Appl. Phys. Lett.* 96, 18 (2010).
46. K. Lipert, M. Ritschel, A. Leonhardt, Y. Krupskaya, B. Büchner, and R. Klingeler, *J. Phys. Conf. Ser.* 200, 072061 (2010).
47. X.G. Sun, M. Gao, C. Li, and Y. Wu, *Microwave Absorption Characteristics of Carbon Nanotubes*, ed. S. Yellampalli (Europe: In Tech, 2011), pp. 265–278.